SSIM 2023 – PM Dight (ed.)

doi:10.36487/ACG_repo/2335_40

A hybrid deterministic–stochastic discrete fracture network to evaluate potential inter-ramp instabilities

P Edmondson *WSP, Australia*

S Rogers *WSP, Canada*

Abstract

The rock mass at Batu Hijau is characterised by the presence of major and intermediate scale faulting that impacts slope stability at the inter-ramp scale. This was identified as the key element for any anticipated failure mechanism during the next phase of the open pit development. Traditional kinematic analyses of planar (one sliding face) and wedge (two sliding faces) failures are carried out at the inter-ramp scale to assess stability based on prescribed Factor of Safety (FoS) and Probability of Failure (PoF) measures.

This case study used a full 3D discrete fracture network (DFN) modelling approach, carried out within the FracMan® code, to fully evaluate inter-ramp scaled instabilities. The analysis technique uses a limit equilibrium approach to consider the stability of complex polyhedral wedges formed within the slope from both explicit wireframed structures and stochastically generated intermediate scale structures. The explicit wireframe structures are based on the deterministic fault model from mapping over life of mine. The stochastic faults were developed based primarily upon parameter inputs from acoustic televiewer (ATV) surveys obtained when drilling in the walls for the next stage of mining.

For each realisation, the deterministic (explicit) major faults were combined with the stochastically generated intermediate scale faults to create a far more realistic description of the slope rock mass fabric in the form of a DFN model. The DFN is then searched for potential wedges, with both planar and wedge failing blocks being identified. A composite mechanism was explored by checking stability on non-daylighting wedges using the limit equilibrium tool.

Key model input variables were calibrated to match failure volumes recorded from the previous stage of mining. The same variables were then projected onto the future mining stage to predict future failure volumes. Based on the anticipated structure, comparable results were obtained for blocks greater than 1,000 m³, considering the larger size of the next mining stage. Results provided a more realistic prediction of how the rock mass fabric contributed to instability and gave confidence to optimising slopes at the mine.

Keywords: *discrete fracture network, complex kinematics, limit equilibrium tool, Probability of Failure, Factor of Safety*

1 Introduction

Batu Hijau is a large copper porphyry deposit located on Sumbawa, Indonesia, where production commenced in 2000. The open pit at the time of study was at the end of phase 6/beginning of phase 7, with walls approaching 800 m deep. Phase 7 design had been confirmed during previous work and a phase 8 concept had been approved. The design work undertaken was part of the confirmation of phase 8 to a feasibility level of study and was based on 6,000 m diamond core drilling, material sampling, testing and characterisation work. Geotechnical analyses for slope design included use of both limit equilibrium (LE) and finite element methods.

A discrete fracture network (DFN) was developed to better understand the complex interaction between the structure. The DFN was analysed using complex kinematics (rock block identification) and LE techniques (Rogers et al. 2018) to assess instability based on Factor of Safety (FoS) and Probability of Failure (PoF).

The workflow outline is described in Figure 1.

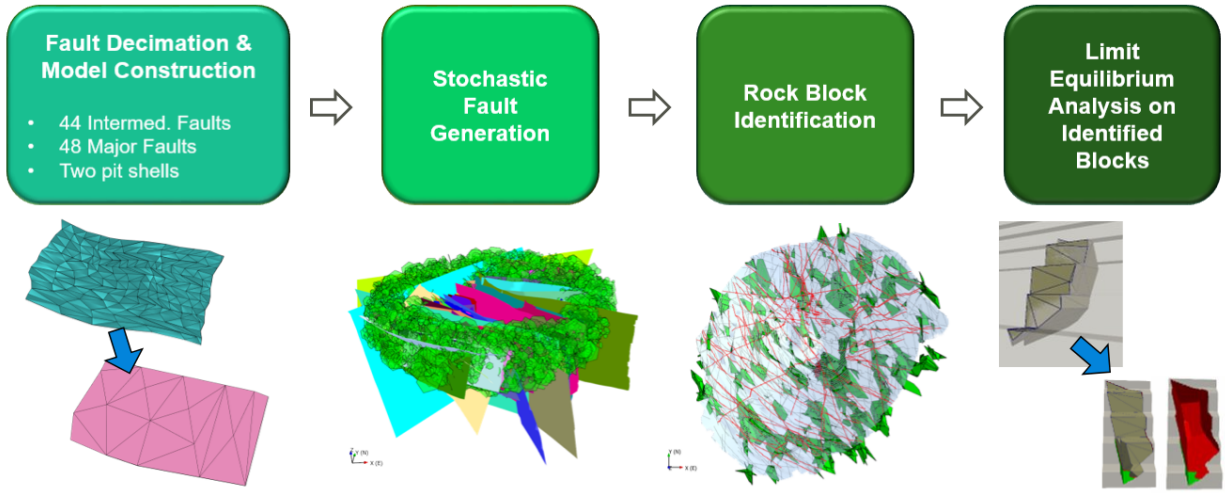

Figure 1 Workflow outline adopted for the DFN-LE-tool assessment

2 Discrete fracture network development

The rock mass at Batu Hijau is characterised by the presence of northeast and west-northwest trending lineaments which may represent arc parallel and arc normal structures associated with tertiary subduction (Meldrum 1994), and which were the basis of the DFN.

2.1 Mapped faults (deterministic)

Large-scale structure which had been mapped over life of mine was considered high confidence and was therefore modelled deterministically. Wireframes were available for these structures, as shown in Figure 2. A key assumption was they were considered persistent over the phase 8 pit shell.

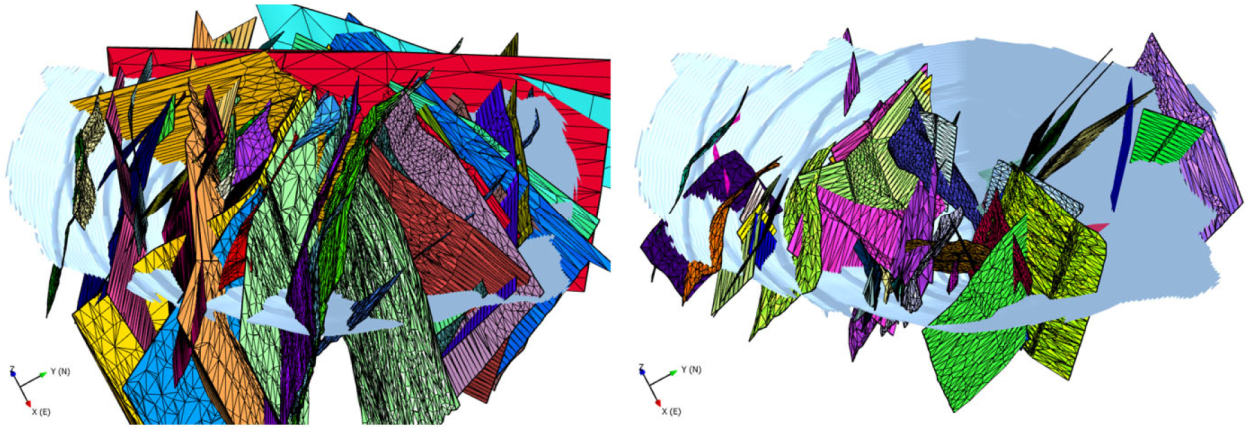

(a) (b)

Figure 2 Mapped wireframes structures: (a) Major structure; (b) Intermediate structure

2.2 Acoustic televiewer faults (stochastic)

A large portion of structure identified through ATV survey (95%) are small-scale joints and fractures not considered critical to inter-ramp stability as they are non-persistent. Larger structures including faults and shears with medium and high confidence status were selected. ATV data used for generation of the DFN is shown in Figure 3, which indicates more spread than the mapping data, although this could be a processing issue.

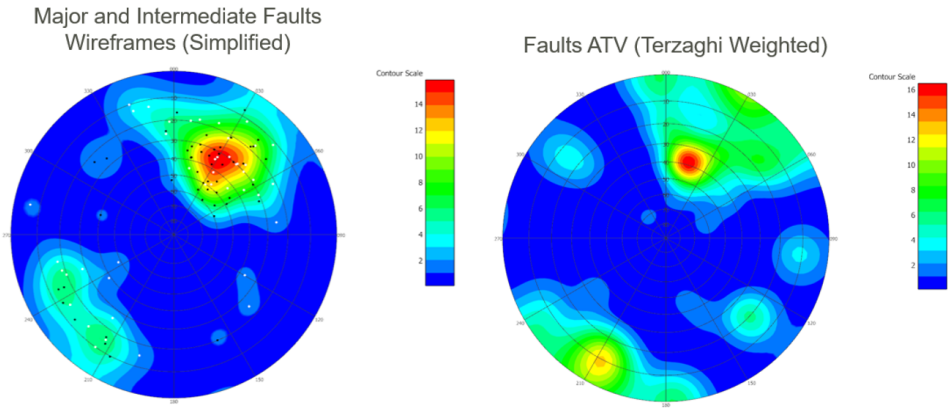

Figure 3 Wireframe (mapped) faults compared to ATV faults

2.3 Stochastic fault input parameters

2.3.1 Orientation

Orientation data are available from the fault wireframe objects and from observed feature types in the ATV data. Stereonet analysis was carried out on the available data to provide a basis for generating stochastic fault orientations. Bootstrapping was used to generate stochastic orientations based upon multiple random sampling, with replacement and dispersion from an original sample used to create a pseudo-replicate sample of fault orientations (Efron 1979). Terzaghi weighting was applied to reduce the impact of drilling bias.

2.3.2 Fault size analyses

The length distribution of the modelled fault objects was considered in order to constrain the size of smaller stochastic faults. The trace length of wireframe structures was plotted using a power law analysis technique at multiple elevations within the project area (Figure 4). Power law analysis reflects the common observation that many geological structures show scale invariant properties over large-scale ranges. The power law trend is then interpreted and used to constrain the size distribution of stochastic small-scale faults.

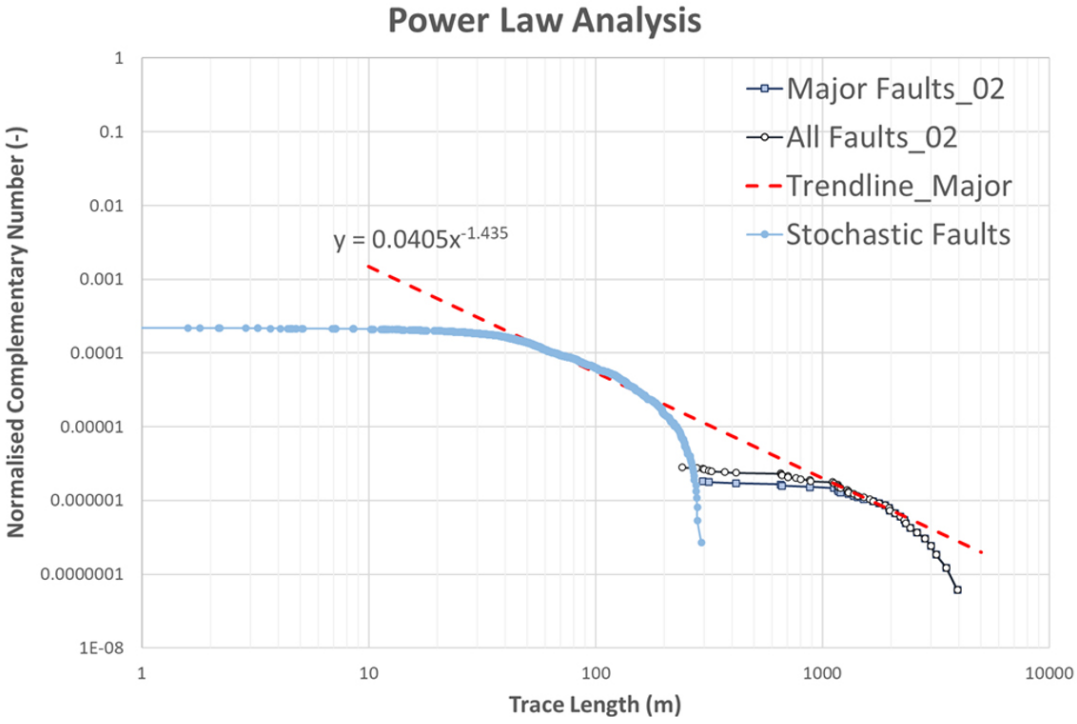

Figure 4 Power law analyses on simulated faults

2.3.4 *Fault intensity analyses*

Discontinuity intensity was undertaken initially by calculating fracture type per unit length (P10) and then converting it to a volumetric estimate of fracture area per unit volume (P32) using the Chiles et al. (2008) method. Summary statistics and histograms for P10 and calculated P32 values for faults are provided in Figure 5.

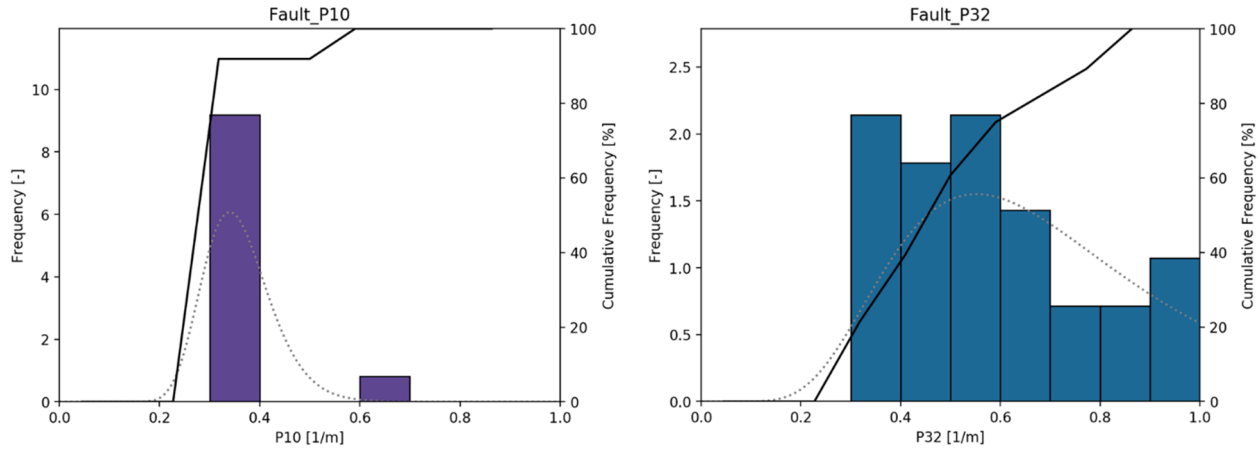

(a) (b)

Figure 5 Distributions of (a) measured P10 intensity and (b) computed P32 intensity

2.3.5 *Volumetric intensity and distance to fault*

A broad trend was noted between P32 intensity and distance to mapped major faults, with P32 intensity reducing with increasing distance from these faults. The relationship is quite noisy when the raw data are viewed and can be more clearly seen by binning the data into fixed distance windows. P32 used as this represents a more directionally independent isotropic intensity measure (Figure 6).

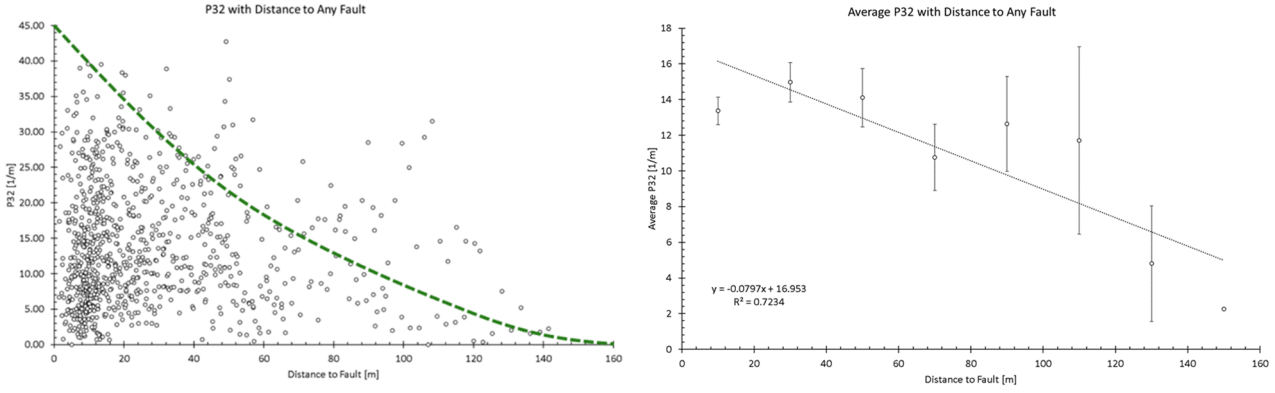

(a) (b)

Figure 6 Relationship between P32 and distance to fault: (a) Raw data; (b) Chart binned data

Using the developed relationship between P32 and fault distance, P32s were populated within the grid using a minimum of 0/m and maximum of 50/m. The distribution of P32 in the grid is similar to the distribution of P32 estimated on the ATV intervals and is used to determine local fault potential at that grid cell location. The P32s in the grid were scaled to achieve a better match between the estimate ATV P32s. The mean of the ATV data (13.54/m) normalised by the mean of the original grid calculated values (11.02/m) was used as a scaling factor (1.23). Each P32 value in the grid was multiplied by this factor (Figure 7).

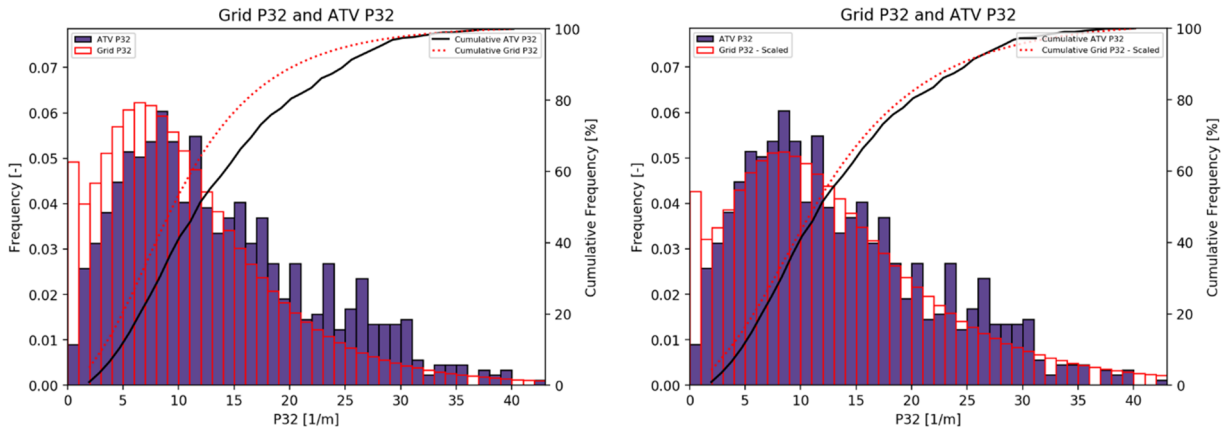

(a) (b)

Figure 7 (a) Comparison between Grid P32 and ATV P32; (b) Scaled grid

2.4 Stochastic fault generation

The inputs for stochastic fault generation are outlined in Table 1. Stochastic faults were generated within 300 m of the pit surface to improve computation times. Structures beyond this limit are unlikely to have any influence on stability as they will be locked in by high confinement stresses as well as their likely geometry.

Table 1 Stochastic fault properties

Property	Constrained by	Values
Fault orientation data	Orientation bootstrapped from wireframe faults using inverse distance relationship	Bootstrapped with dispersion of k = 80
Fault intensity data	Intensity defined by the average logged ATV fault intensity (scaled for size truncation)	Average fault P32 = 0.72 m-1 After scaling P32 = 0.029 m-1
Fault size data	Power law size analysis	Gradient 1.435, min 20 m maximum 150 m

The traces for the mapped major and intermediate (wireframe) faults and stochastic faults generated from the DFN are projected onto the phase 8 pit design as shown in Figure 8. Typically, the stochastically generated faults are at a scale in between the major deterministic faults and joints which will impact stability at the inter-ramp scale.

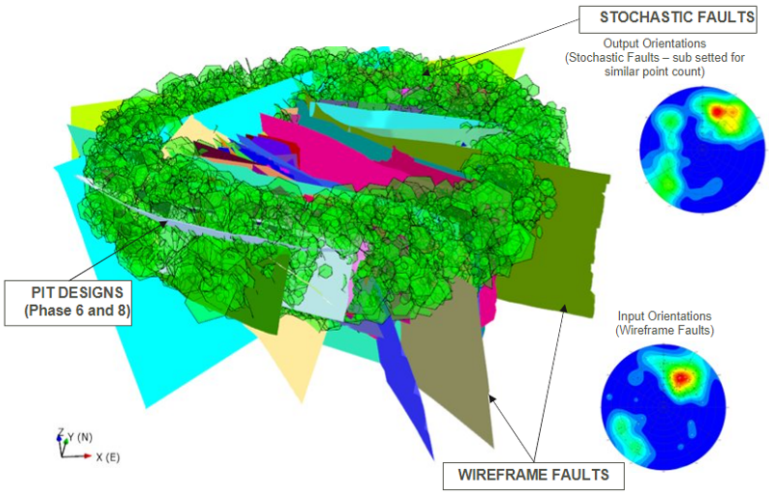

Figure 8 Deterministic (mapped wireframes) and stochastic fault traces mapped onto the phase 8 design

3 Geotechnical analyses

The geotechnical assessment involved running the 3D complex wedge tool within FracMan® (WSP 2023) to identify rock blocks. Non-daylighting wedges were analysed using 3D PoF, based on the method of Lawrence et al. (2020), which computes a FoS on each block based on an LE approach (Valerio et al. 2020). These methods are computationally fast and allow large number of iterations to be performed relatively quickly. Input material parameters were calibrated based on phase 6 failure volumes and then applied to the phase 8 assessment.

3.1 Pit shells

A key element of the assessment is the calibration of the model against the phase 6 site-recorded failure volumes, which were typically above bench scale (multi-batter to inter-ramp). Phase 6 and phase 8 pit shells are shown in Figure 9, with benches removed for ease of analysis. Pit sector analysis was based on historical performance, with sectors shown in Figure 10.

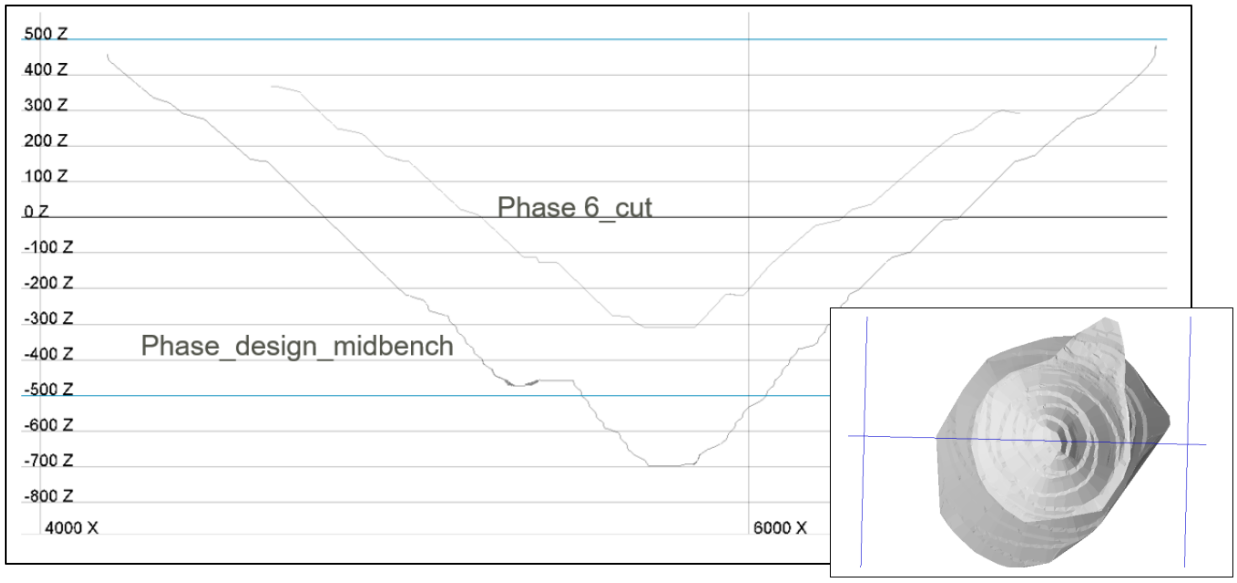

Figure 9 Pit shells used for the assessment (phase 6 and phase 8)

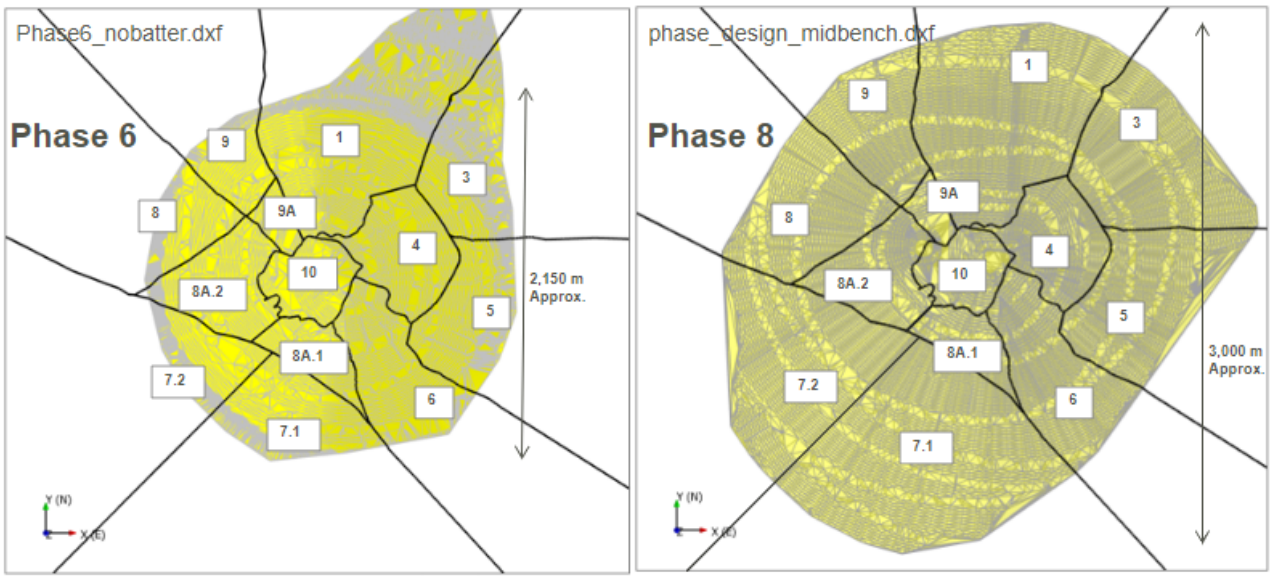

Figure 10 Pit sectors used in analysis

3.2 Material properties

A range of input properties were selected based on statistical distributions identified during the phase 8 characterisation work. Pore pressure was applied based on the Ru method with a range between 0 and 0.4. A summary of the input properties is presented in Table 2.

Cases	Scenarios	Rock density	Joint strength		Rock strength				Pore pressure
		Unit weight (KN/m³)	Cohesion (kPa)	Friction angle (deg)	UCS (MPa)	GSI	m_i	Disturbance factor (D)	Ru
Base case	1–8	26.5	0	30	98	62	26	0.7	0–0.40
Low discontinuity strength	9–17	26.5	0	20	98	62	26	0.7	0–0.40
Low rock mass strength	18–26	26.5	0	30	59	45	15	1.0	0–0.40
Low discontinuity and rock mass strength	27–35	26.5	0	20	59	45	15	1.0	0–0.40

Table 2 Material properties adopted for analyses

3.3 Rock block identification

Planar and wedge type mechanisms are identified within FracMan's kinematic wedge tool. Non-daylighting blocks held stable by a buttress of rock mass or concave geometries are also identified as per Figure 11. A filter was used to only include blocks found less than 100 m below the pit wall surface. This was deemed realistic based on historical depth of failure, and anything else was discounted from the analyses.

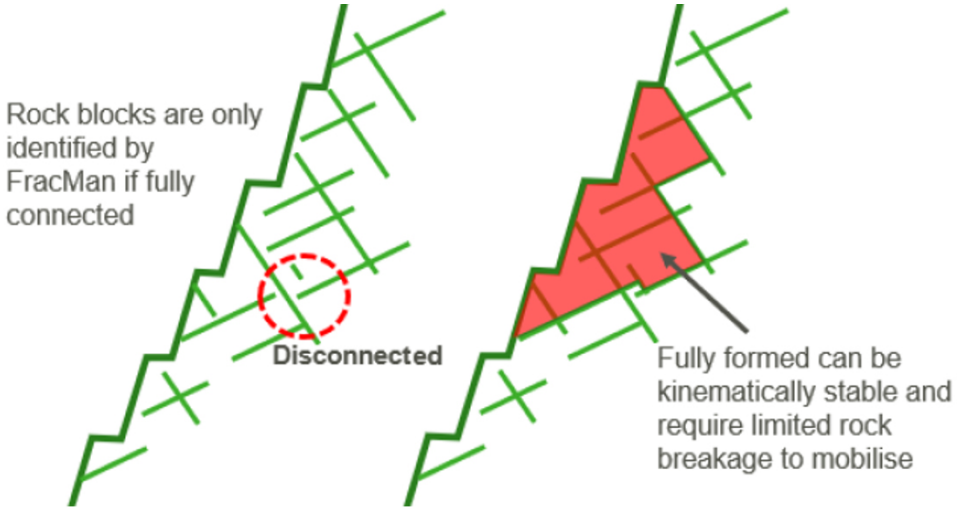

Figure 11 Rock block identification

3.4 Results

3.4.1 Phase 6 calibration

Results of the sector analyses (sector 3) for phase 6 are presented in Figure 12, which shows the strength cases and pore pressure conditions required to simulate failure volumes recorded during phase 6. These conditions were then projected onto the phase 8 assessment.

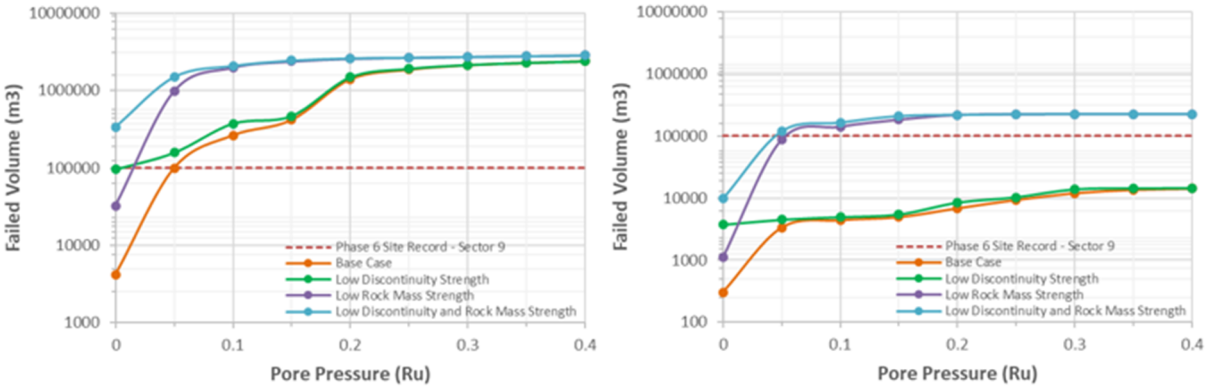

Figure 121 Results of (a) phase 6 sector 9 (Example A) and (b) phase 8 sector 9 (Example B) showing conditions required to produce site-recorded failure tonnages

3.4.2 Phase 8 results

Results are shown in Table 3 and plotted visually to assess the spatial distribution of blocks in Figure 14.

Table 3 Results-predicted volumes for calibrated phase 8

Sector	Phase 6 failed volume (m^3)	Conditions to meet phase 6 failed volume	Phase 8 predicted failed volume (m^3) (a) and PoF% (b)	Comments
1	140,835 (3%)	Base case, Ru 0.2	49,300 (12%)	
3	79,434 (4%)	Low discontinuity strength, Ru 0.2	4,190 (28%)	
4	249 (0%)	No observed provided-assumed target base case, Ru 0.15 (c)	65 (<0.5%)	Low simulated volume for both pit shells
5	167,718 (9%)	Base case, Ru 0.1	7,140 (15%)	
6	2,471 (<1%)	Base case, Ru 0.2	225 (<0.5%)	Slight underestimate – actual observed was at ~Ru = 0.21
7	93,625 (5%)	Low discontinuity and rock mass strength, Ru 0.2	9,620 (8%)	
8	111,990 (4%)	Low rock mass strength, Ru 0.2	2,000 (3%)	
8A	126,310 (2%)	Base case, Ru 0.1	280 (1%)	Slight underestimate – actual observed was at ~Ru = 0.12

Sector	Phase 6 failed volume (m^3)	Conditions to meet phase 6 failed volume	Phase 8 predicted failed volume (m^3) (a) and PoF% (b)	Comments
9	99,248 (3%)	Base case, Ru 0.05	3,333 (1%)	
9A	61 (0%)	No observed provided-assumed BC 0.05 (c)	7,750 (4%)	Low simulated volume for both pit shells
10	4,568 (2%)	Low discontinuity and rock mass strength, Ru 0.15	490 (11%)	

	Decrease from Phase 6 (of unstable volume)
	Increase from Phase 6 (of unstable volume)

a) Average Unstable Volume Per Realization (i.e., cumulative results / 100 realizations)
b) POF = Probability of Failure (Unstable Volume/Cumulative Volume)
c) Sector 4 uses an "observed volume" from the average of neighbouring sectors 3 and 5, Sector 9A uses an "observed volume" from Sector 9

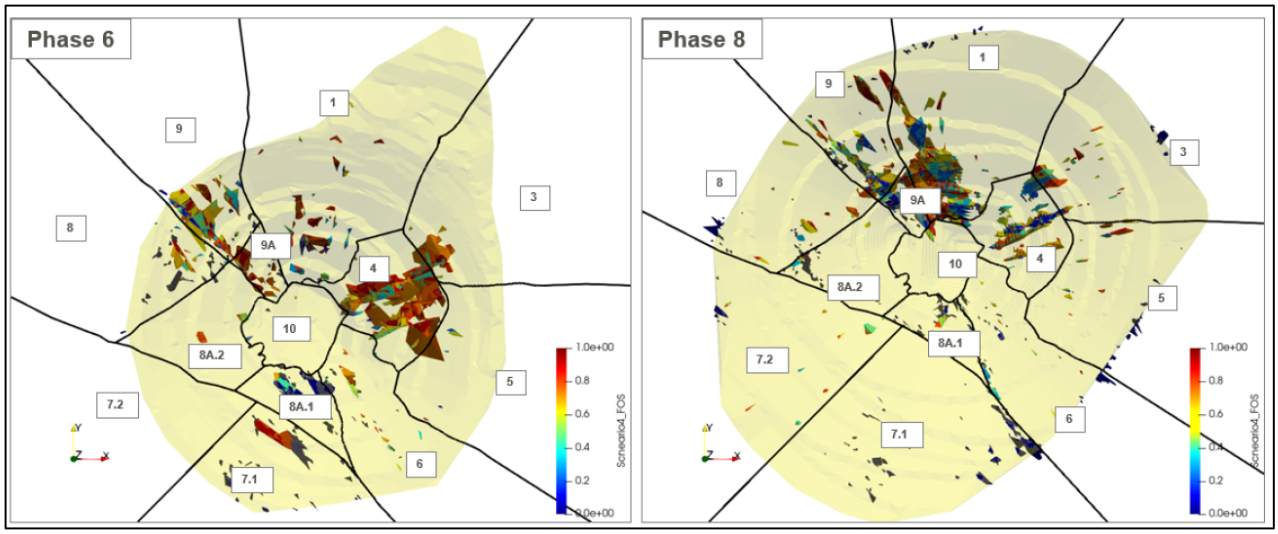

Figure 14 Failed blocks base case strength at Ru = 0.2

4 Discussion

Failure volumes are generally lower for the phase 8 shell, though they should be assessed in conjunction with PoF. The observed failure volume from failure tonnage records is simulated on the phase 6 pit in all sectors except 7. Low rock mass strength and increased pore pressure is required to achieve the observed failure in sector 7. Pore pressure is seen to have an immediate effect on stability in the phase 6 pit in Example A. Nearly the entire average cumulative volume (~2.9 million m^3) has become unstable for all cases at Ru = 0.2. There is a smaller range in the base case phase 8 (Example B) failure volumes when compared to phase 6. This indicates that a significant number of blocks are locked in (i.e. failure through rock mass is required) and will not be affected by variations of pore pressure.

Limitations of the study include that both designs were assessed without the bench detail so may lack accuracy, and blocks greater than 100 m below the surface were excluded as they were deemed unrealistic based on historical depths of failure.

The generation of a hybrid DFN that combines a high confidence deterministic fault model with a stochastic model allowed a range of possible scenarios to be explored quickly and efficiently. Adopting a probabilistic approach has enabled calibration of the model to a previous mining stage, thereby improving confidence in the results. A stronger focus on structure and or a composite mechanism is a better match to reality compared to traditional continuum approaches. The results provided confidence in the slope design and resulted in optimisation at the mine.

Acknowledgement

The authors would like to thank AMNT for its support and collaboration on this project, and its permission to publish the work.

References

Chiles, J, Wackernagel, H, Beucher, H, Lantuejoul, C & Elion, P 2008, 'Estimating fracture density from a linear or aerial survey', *Proceedings of the VII International Geostatistics Congress*, pp. 535–544.

Efron, B 1979, 'Bootstrap methods: another look at the jackknife', *The Annals of Statistics*, vol. 7, no. 1, pp. 1–26.

Lawrence, KP, Nelson, M, Yetisir, M & Matlashewski, P 2020, 'Kinematic assessment of composite failure mechanisms in pit slopes: a novel slip surface identification algorithm for DFN models', *Proceedings of the 54th US Rock Mechanics Symposium*, American Rock Mechanics Association, Alexandria.

Meldrum SJ 1994, 'The Batu Hijau porphyry copper-gold deposit, Sumbawa Island, Indonesia', *Journal of Geochemical Exploration*, vol. 50, no. 1–2, pp. 203–220, https://doi.org/10.1016/0375-6742(94)90025-6

Rogers, S, D'Ambra, S, Dershowitz B & Turnbull, R 2018, 'Probabilistic bench scale slope designs based upon realistic discrete fracture network models', *Proceedings of the 2018 International Symposium on Slope Stability in Open Pit Mining and Civil Engineering*, BCO Congresos, Barcelona.

Valerio, M, Rogers, S, Lawrence, KP, Moffitt, KM, Rysdahl, B & Gaida, M 2020, 'Discrete fracture network based approaches to assessing inter-ramp design', in PM Dight (ed.), *International Symposium on Slope Stability in Open Pit Mining and Civil Engineering, Australian Centre for Geomechanics*, Perth, pp. 1017–1030, https://doi.org/10.36487/ACG_repo/2025_67

WSP 2023, FracMan®, version 8.1, computer software, https://www.wsp.com/en-us/services/fracman/